MEDWIN PUBLISHERS
Committed to Create Value for Researchers

Petroleum & Petrochemical Engineering Journal
ISSN: 2578-4846

Silica-Rich Intervals Characterization Based on Acoustic Borehole Image and Elemental Capture Spectrometry Integration: A Case Study from Barra Velha Formation, Santos Basin (Brazil)

de Jesus IL[1,2]*, Abrantes Jr. FR[2,3] and Lupinacci WM[2,3]

[1]Reservoir Research Group (PETROCARB), Observatório Nacional (ON), Brazil, ORCID: 0000-0002-0599-2104

[2]Exploratory Interpretation and Reservoir Characterization Group (GIECAR), Universidade Federal Fluminense (UFF), Brazil, ORCID: 0000-0002-3801-7532

[3]National Institute of Science and Technology of Petroleum Geophysics (INCT-GP/CNPq), Brazil, ORCID 0000-0002-5728-7423

Research Article

Volume 10 Issue 3

Received Date: July 08, 2026

Published Date: August 05, 2026

DOI: 10.23880/ppej-16000418

***Corresponding author:** Igor Lima de Jesus, Reservoir Research Group (PETROCARB), Observatório Nacional (ON), Rio de Janeiro, Brazil, ORCID: 0000-0002-0599-2104

Abstract

Silicification is a common diagenetic process in Aptian Pre-Salt carbonate successions, characterized by the replacement of carbonate minerals by silica, with implications for reservoir quality. This study presents an integrated methodology combining borehole image logs, elemental capture spectroscopy, and petrographic thin-section analysis to evaluate silicification effects on the permoporous properties of the Barra Velha Formation, Santos Basin. The vertical distribution of silica volume derived from well logs allowed the subdivision of the Barra Velha Formation into five intervals (S1–S5). These intervals were associated with permoporosity data to establish a relationship between silicification and reservoir properties. The results reveal a progressive upward increase in silicification throughout the formation, accompanied by a corresponding decrease in permoporous properties. In contrast, localized intervals exhibiting both high silica content and enhanced permoporosity were identified as anomalous zones, indicating that silicification does not uniformly degrade reservoir quality. The combined petrophysical and petrographic analyses suggest that silica migration and accumulation were driven by hydrothermal silica-rich fluids ascending through fractures and faults. These fluids promoted calcite dissolution, generated secondary porosity, while simultaneously precipitated silica that partially or completely cemented pore spaces. Consequently, silicification exerted a dual influence on the Barra Velha reservoir, locally enhancing porosity through dissolution but, overall, reducing reservoir quality through silica cementation. These findings demonstrate the value of different petrophiscal and petrographic data to characterize silicification impact and improve the understanding of diagenetic controls on the permoporous quality of Pre-Salt carbonate reservoirs.

Keywords: Silicification; Pre-Salt; Permoporosity; Borehole Image; Nuclear Magnetic Resonance

CC BY

Introduction

In the last decade the oil production in the Santos Basin reached the mark of 2.9 Mboe/day, being responsible for 74% of the national oil production in 2022 [1], (Figure 1A). This achievement was granted due to technology development that favored to succeed drilling and developing wells in deep waters. Besides the relatively simple mineralogy, the Aptian carbonate reservoirs are characterized by depositional and diagenetic processes that result in extremely heterogeneous characteristics [1-4]. Due to the simultaneity of diagenetic processes, their distinction becomes challenging [5,6].

The permeability and porosity of carbonate framework, observed in several pre-salt fields, were reorganized and/or altered due to diagenetic processes [7,8]. Silicification must be highlighted, among these processes, due to its importance in affecting pore dissolution and cementation features, impacting the permoporous properties of pre-salt carbonate reservoirs [1,9].

Silicification is a diagenetic process of carbonate rocks, characterized by the replacement of carbonate by silica (SiO4-opal and quartz) and, consequently, the precipitation of pore-filling silica cement [10,11]. The Barra Velha Formation (BVF) deposits are dated from Aptian. Although originally interpreted as a marine setting [12,13], they are, recently, interpreted as an alkaline lake environment [14-17]. The BVF comprises laminites, shrubs and spherulites [18] and presents reservoirs of excellent quality [19].

This work aimed to identify different silica zones based on the distribution of the Si content patterns observed in the BVF. It integrated the acoustic borehole image, elemental spectrometry and thin section data to identify features that may be related to diagenetic processes.

Geological Setting

The infilling of the Santos Basin initiates during the Gondwana supercontinent rupture through the Late Jurassic-Early Cretaceous transition [12,13]. Its genesis is associated with extensional tectonic efforts, which consequently developed the Atlantic Ocean and caused the separation of the South American and African continents [12]. This rupture occurred over a complex of cratonic blocks of the Paleoproterozoic-Archaean age and Neoproterozoic orogenic belts [12,19]. The rifting processes that allowed the formation of the marginal basins of the South Atlantic were preceded by a significant outflow of tholeiitic basaltic magma, developing a large Paraná-Etendeka Igneous Province [6,14,20,21].

Regarding the dynamics of the opening of the Atlantic Ocean, Szatmar, et al. [19] propose that this opening occurred almost synchronously along its length, approximately 145 Ma ago (Jurassic-Cretaceous boundary). However, the northwest portion would have remained closed for a slightly longer period, between 145 and 113 Ma (Lower Cretaceous). This asynchronous behavior between the two portions generated a wedge shape, with a widening in the southern region. For the authors, this lack of synchrony in the opening is associated with a rotation induced by the rise of the mantle flow, just below the opening rift. The genesis of this province is associated with the progression of the rift, so that the fault reached the subcontinental lithospheric mantle, with high temperatures, which allowed widespread melting. However, the authors consider that this extrusion occurred in alternation with sedimentation until 113 Ma. This formation is characterized by basaltic flows from the Lower Cretaceous, which allows the correlation to the age of the flows proposed by Szatmari, et al. [19].

Moreira [12] separates the sedimentary record of the Santos Basin from erosional unconformities associated with the main phases of tectonic evolution, characterizing three supersequences: (i) rift, (ii) post-rift, and (iii) drift. The Rift Supersequence comprises a mosaic of synthetic and antithetical faults with a NE/SW direction and encompasses the Camboriú, Piçarras, and Itapema formations. The Camboriú Formation, interpreted as an economic basement, is composed of dark gray-colored, holocrystalline basalts made up mainly of plagioclase and pyroxene. The Piçarras Formation is characterized by terrigenous sediments deposited discordantly on the basalts of the Camboriú Formation during the Barremian Age [12]. It is characterized by conglomerates, possibly related to alluvial fans of the proximal areas, and talc-stevensite shales and siltstones corresponding to distal lacustrine sediments. The Itapema Formation ends the Rift Supersequence (Upper Barremian-Lower Aptian). This formation is limited at its base by the pre-Jiquiá unconformity (Figure1b) and, at its top, by the Pre-Alagoas unconformity. The sequence characterized by intercalations of calcirrudites composed of fragments of pelecypod shells and dark shales rich in organic matter occur in the distal portions. In the proximal portions, records of alluvial fans of conglomerates and sandstones are observed [12,19,22,23].

The Post-Rift Supersequence comprises Upper Aptian sediments with relative tectonic quiescence. Its sedimentation is interpreted as transitional between the continent and shallow marine, characterized by the Barra Velha and Ariri formations [12]. The Barra Velha Formation is divided into two main sequences: lower and upper. The Intra-Alagoas Unconformity (117 Ma) separates the sequences, commonly mapped as a regional reflector. The top of the Barra Velha Formation is characterized by evaporites that delimit the beginning of the transitional-marine evaporite environment. These evaporites (Ariri Formation) were

Copyright© de Jesus IL et al.

deposited in the Neoaptian. This period expresses intense aridity, which allowed the deposition of a thick package (up to 2,000 meters) of evaporites. In general, evaporites are composed of halite and anhydrite. However, other salts are also recorded, such as tachydrite or carnallite [5,22]. The Drift Supersequence encompasses sediments deposited from the Albian to the Recent. In this context, a character of thermal subsidence is observed that can be related to the evolution of the passive margin of the Santos Basin [12].

In divergence from the aforementioned proposals, Wright, et al. [24] establish a division for the Barra Velha Formation, based on the Intra-Alagoas unconformity, where the lower portion of the formation should be interpreted as a rift phase, while the upper portion denotes a sag phase (Figure 1B), The authors identify a separation of the rift phase, limited by the pre-Alagoas unconformity, so that the Piçarras and Itapema formations are associated with the lower portion, while the upper portion of the rift phase encompasses the limestones of the Barra Velha Formation, deposited up to Intra-Alagoas unconformity (Figure1B). This model, defined by Wright [25] has been adopted by different authors in recent publications on the Santos Basin [1,2,3,5,15,16,17,26,27,28,29,30] and it is used in this work.

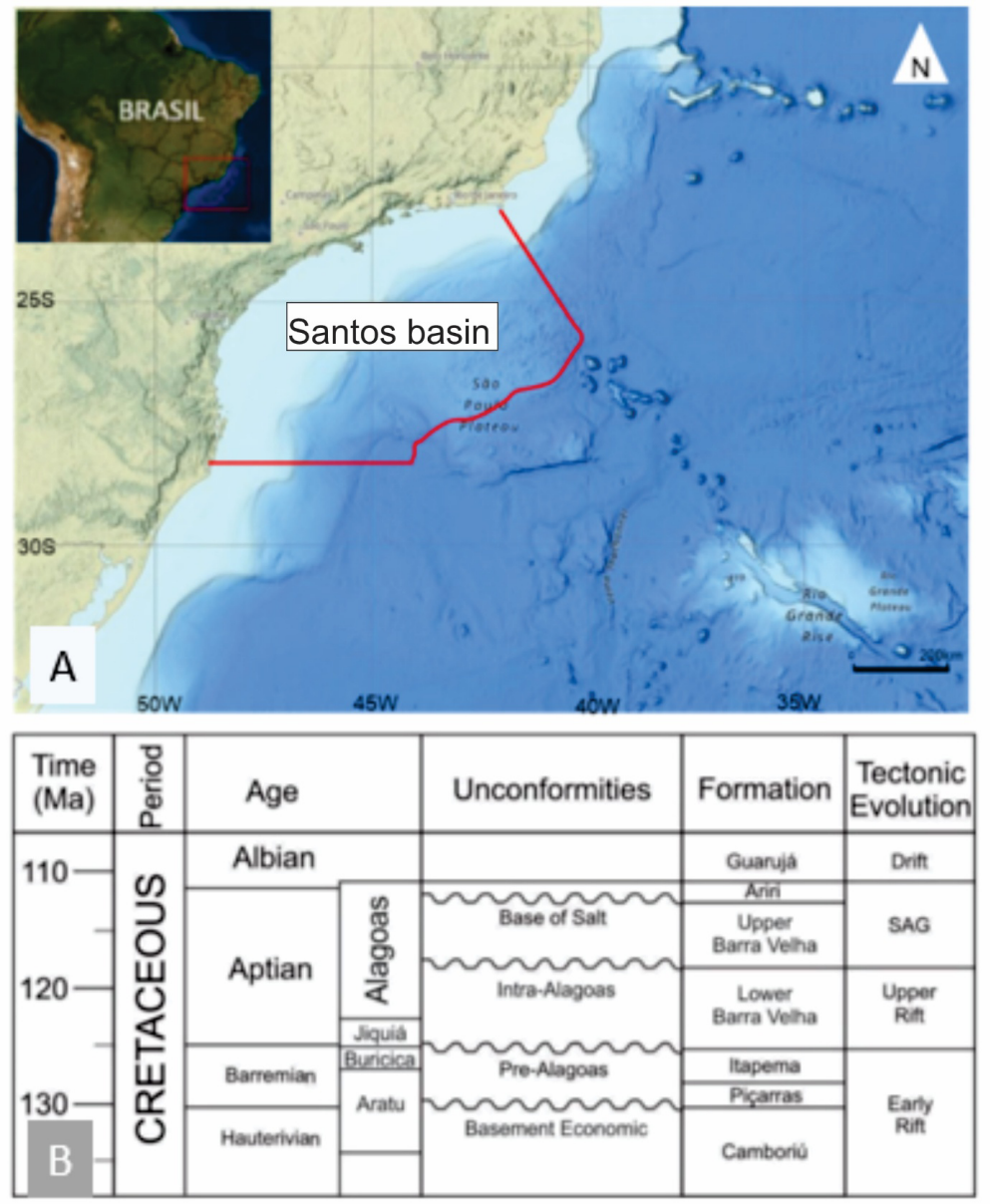


Figure 1: A) Location map of the Santos Basin; B: Schematic illustration of tectono-stratigraphic evolution of the Santos Basin (after [12,18]).

Copyright© de Jesus IL et al.

Materials and Methods

The silica zones or intervals of the Barra Velha Formation (BVF) were studied in one well from a pre-salt field, named here as Well A. The succession analyzed comprises the entire BVF. The well-log data were provided by Agência Nacional de Petróleo (ANP). The following well-logs were considered: gamma-ray (GR), caliper (HCAL), calcite, silica and dolomite volumes, T2 distribution, porosity and permeability from NMR, thin section descriptions, and Acoustic Borehole Images (BHI). Based on Si, Ca, and Mg content, concentrations measured from the Elemental Capture Spectroscopy tool (ECS), it was possible to estimate silica, calcite, and dolomite volumes by converting the element's proportion in lithological volume considering molecular weight and elements ratio [1,31]. Table 1 displays the element's weight and the element ratio of the Barra Velha formations' main lithologies.

Mineral	Chemical Formula	Molecular weight	Elements ratio	Sum
Quartz	SiO_2	60.08gm	Si:46,74% O: 53,26%	100%
Calcite	$CaCO_3$	100.09gm	Ca:40,04% C:12,00% O: 47,96%	100%
Dolomite	$CaMg\ (CO_3)^2$	184.40gm	Ca:21,73% Mg: 13,18% C: 13,03% O: 52,06%	100%

Therefore, the silicon (Si) conversion into silica is established by equation 1 (Equation 1).

$$\text{Silicification}=\frac{\text{Si}}{0.4674} \quad (1)$$

In turn, the magnesium (Mg) conversion into dolomite is established by equation 2 (Equation 2).

$$\text{Dolomitization}=\frac{\text{Mg}}{0.1318} \quad (2)$$

To estimate the calcite volume, it is important to highlight that dolomite also contains calcium (Ca). Therefore, it is necessary to discount the calcium in dolomite so that the volume of calcite is not overestimated. Dolomite has 21.73% Ca. Thus, the calcium in dolomite can be expressed by equation 3 (Equation 3).

$$\text{Dolomite}=\frac{\text{Ca}}{0.2173} \quad (3)$$

Equations 2 and 3 describe the calcite volume of dolomite, which can be expressed by equation 4 (Equation 4).

$$Ca_{Mg} = Mg * (1.6487) \quad (4)$$

Finally, it is possible to estimate the calcite volume by equation 5 (Equation 5).

$$\text{Calcite}=\left(\frac{\text{Ca-Ca}_{\text{Mg}}}{0.4004}\right) \rightarrow \text{Calcite}=\left(\frac{\text{Ca-1.6487*Mg}}{0.4004}\right) \quad (5)$$

Acoustic Borehole Images (BHI) are very effective in feature identification due to their high resolution and 100% coverage on the borehole wall. Acoustic BHI contributes to reservoir characterization by mapping different structures such as fractures, dissolution features, or vugs, which are not observed in conventional logs [32]. For this study, BHI data processing considered quality control, tool centralization, and, eventually, artifacts due to drilling. In acoustic BHI, the color scale was standardized: (i) dark colors are associated with low amplitude values, interpreted as porous intervals. (ii) bright colors are associated with higher amplitude and indicate cemented intervals.

After ECS lithology conversion and acoustic BHI processing, based on the silica pattern and behaviors, the BVF was divided into five vertical zones and named upward S1, S2, S3, S4, and S5 (Figure 2). It favored the different diagenetic features identification according to BHI.

Results

The BVF on Well A measures 283 m (Figure 2). The main lithologies found in this well include shrubs, spherulites, and laminites, as well as cherts and dolomites. Packstones, grainstones, and floatstones have been grouped as reworked. The thin section description aims to correlate various types of cement and locate dissolution features. A complementary relationship between calcite and silica volumes can be observed throughout the entire formation. The porosity and permeability values present a decreasing upward trend, while there is an observable increase in silica within the

Copyright© de Jesus IL et al.

same trend.

The S1 zone has a range of 51m (X231.30/X283m). Its lower limit is the Pre-Alagoas unconformity (Figure 2). This zone shows discrete gamma ray (GR) reduction, the lowest silica content, and the highest permoporosity averages of the entire BVF (Figure3). When the BHI is correlated to silica volume, there is an observable increase of silica associated with high amplitude and intercalation of high and low amplitudes. A segment was zoomed in to observe features (Figure 3B) better. As a result, several centimetric pores are bordered by high amplitude, indicating dissolution and intense silicification, partially filling the pore. There are also high-amplitude patches, interpreted as irregular silicification or silica intraclasts [33]. The thin section (X250m) indicates spherulites with dolomite with dissolution pores partially cemented with quartz (Figure 3).

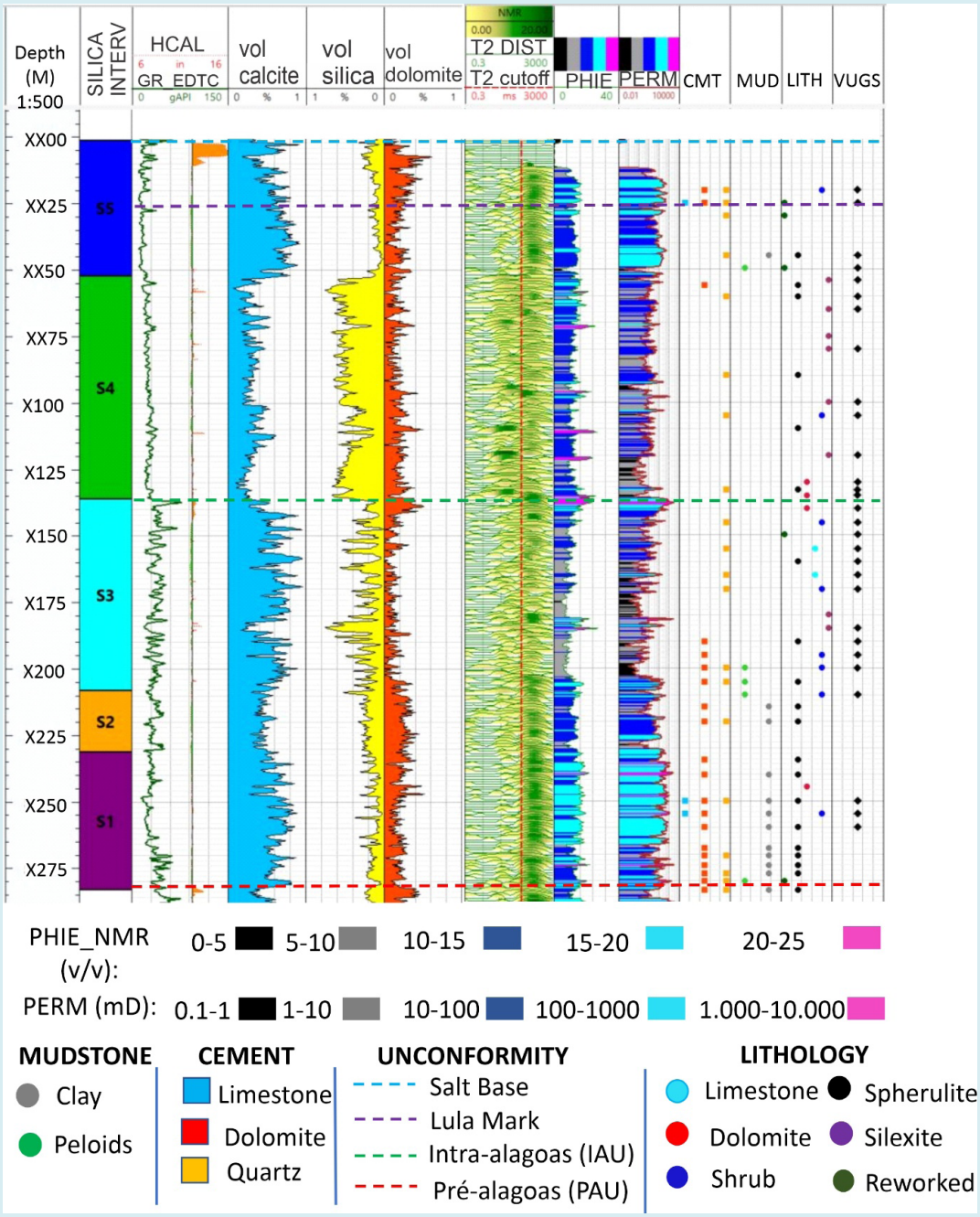


Figure 2: The silica volume zones of the Barra Velha Formation, well-logs and rock data information used in this study.

Copyright© de Jesus IL et al.

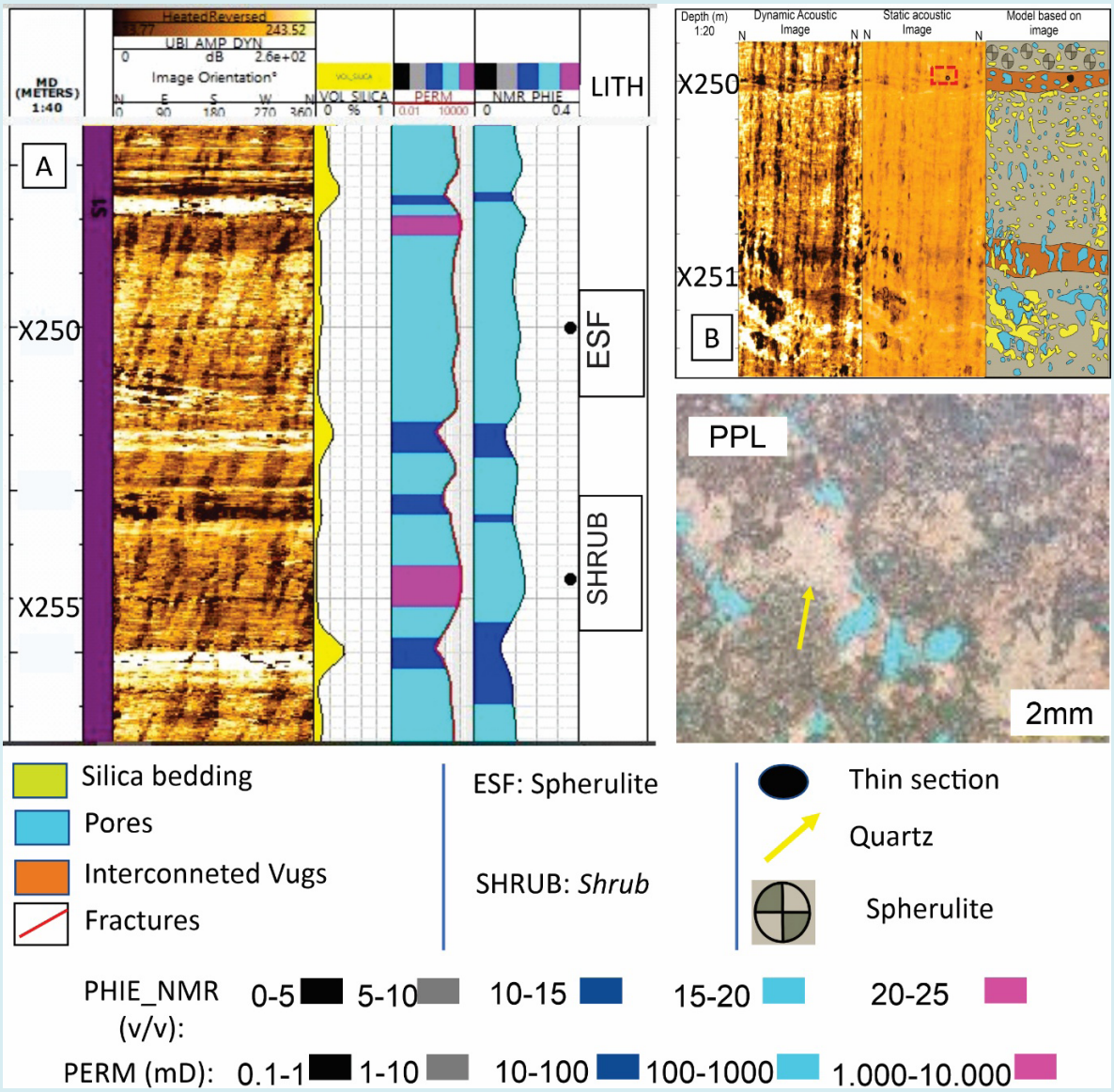


Figure 3: Segment of S1 zone. (A) 1) Depth; 2) Zone; 3) Acoustic BHI; 4) Silica volume; 5) Permeability; 6) Porosity; and 7) Lithology. (B) a zoomed portion, indicated in the blue rectangle, 1) Depth; 2) Dynamic Image; 3) Static Image; 4) Model Based on the image. (C) a thin section image.

The S2 zone has a range of 23m (X208/X231.30m) with lower GR values. An increase in silica volume and a slight decrease in permoporosity is observed when compared to the S1 zone (Figure 2). The silica pattern is uniform throughout this zone. At a depth of X209 m (Figure 4), there is a local increase in silica accompanied by several small-scale fractures in BHI, indicating a brittle behavior. An increase in dolomite volume is reflected as cement in thin sections. The zoomed portion shows two distinct behaviors (Figure 4C): (i) the lower portion is characterized by low to intermediate amplitude, high roughness, and visible porosity interpreted as dissolution, presenting good connectivity reflected in the NMR permeability log, and (ii) the upper portion displays high amplitude with several fractures denoting a brittle behavior and is correlated to high silica volume. Despite the fractures in the upper portion, a decrease in permoporosity is observed when compared to the lower portion (Figure 4). The thin section (X210m) shows shrubs with interparticle porosity partially filled with rhombohedral dolomite and quartz cement, along with some enlarged fractures.

The S3 zone has 51m (X316/X208m) and is characterized by the intercalation of high and low silica values, in a complementary behavior with calcite volume (Figure 2).

Copyright© de Jesus IL et al.

Although this zone presents the lowest dolomite content in the studied succession, there are a few occurrences of dolomite as cement-filling pores. It is important to highlight that the trends of silica increase and permoporosity reduction observed in the previous zones also occur in this zone. However, in some locations, the increase in silica is correlated to an increase in porosity and a reduction in permeability (Figure 5). Silicification seems to have favored dissolution, generating secondary porosity but compromising permeability [1]. The BHI zoomed portion highlights high roughness, intermediate amplitude, and irregular bedding. In the upper portion, the sinusoids are better defined and present a higher amplitude (Figure 5B). The high amplitude patches present diverse geometry and size, interpreted as silica intraclasts [3,33]. Some of the fractures are enlarged, leading to an increase in porosity. The thin section (X185m) is characterized by silexite and sparse spherulites, several vugs, and some enlarged fractures, corroborating the BHI observation (Figure 5C).

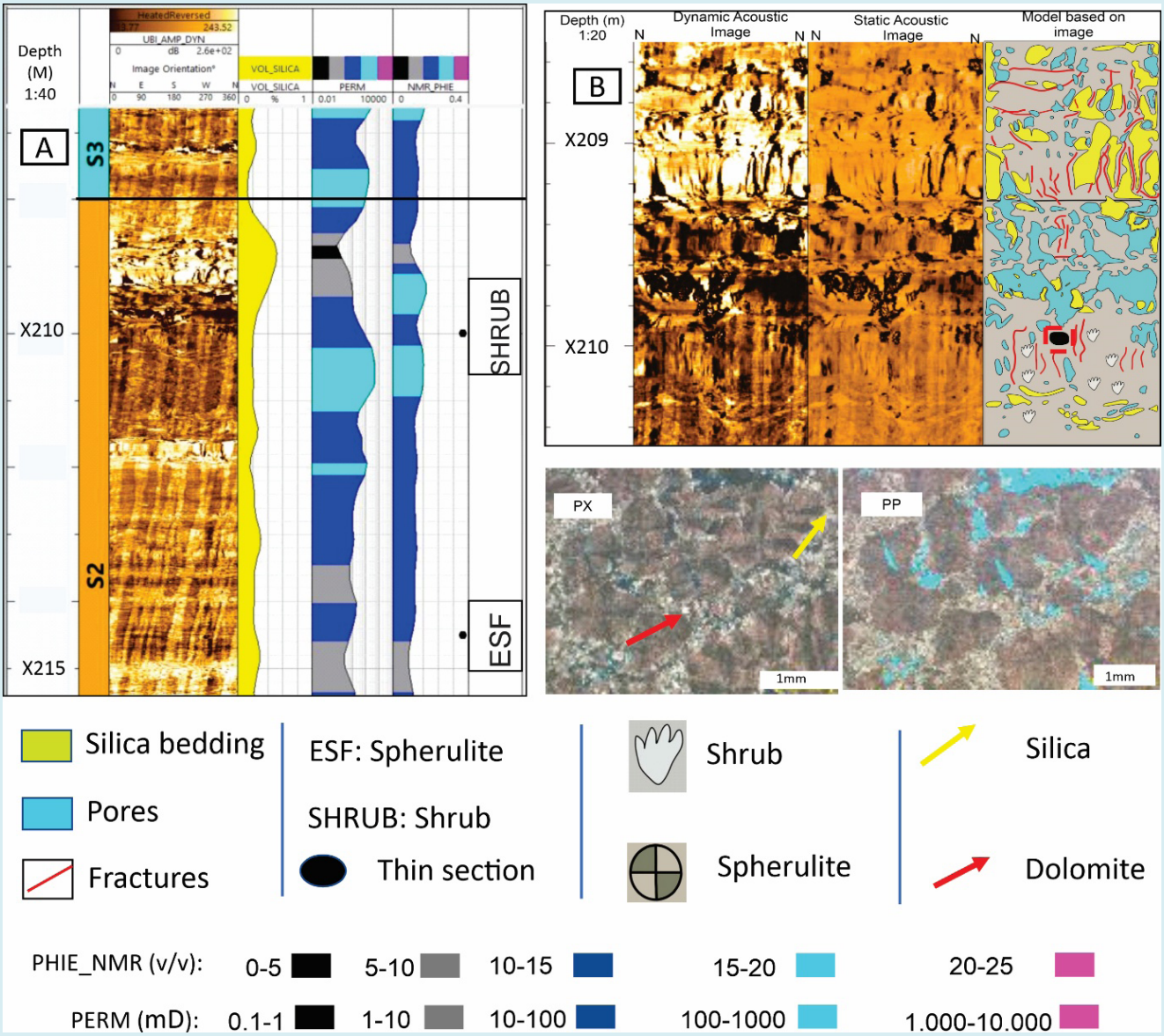


Figure 4: Segment of S2 zone. (A) 1) Depth; 2) Zone; 3) Acoustic BHI; 4) Silica volume; 5) Permeability; 6) Porosity; and 7) Lithology. (B) a zoomed portion, indicated in the blue rectangle, 1) Depth; 2) Dynamic Image; 3) Static Image; 4) Model Based on the image. (C) thin section images.

Copyright© de Jesus IL et al.

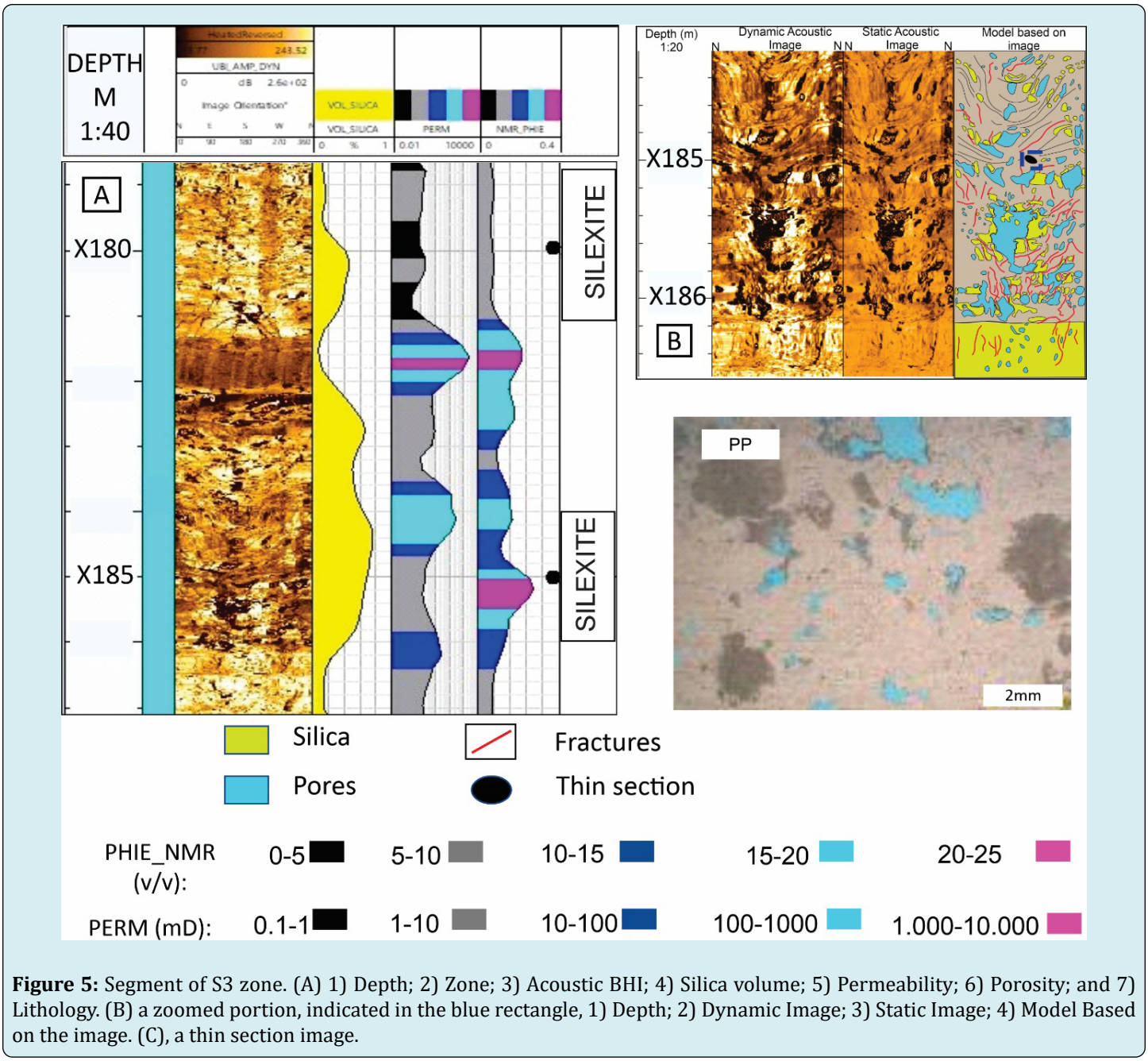


Figure 5: Segment of S3 zone. (A) 1) Depth; 2) Zone; 3) Acoustic BHI; 4) Silica volume; 5) Permeability; 6) Porosity; and 7) Lithology. (B) a zoomed portion, indicated in the blue rectangle, 1) Depth; 2) Dynamic Image; 3) Static Image; 4) Model Based on the image. (C), a thin section image.

The S4 zone is 84m (X052/X136m) and is limited at the base by the Intra-Alagoas Unconformity (IAU; X136m). From the IAU to the top of the zone, the GR shows a slight and continuous reduction trend upwards (see Figure 2). This zone is characterized by an abrupt increase in silica and a corresponding decrease in calcite. Despite the high silica content, the porosity values are like the adjacent zones. In contrast, this interval has the lowest permeability values in the entire BVF. Both BHI analysis and silica content indicate a significant increase in amplitude along the zone, while sporadic intercalations with low-amplitude beddings are still observed. An increase in wide-open fractures along the zone is also noted, which promotes the creation of secondary porosity (Figure 6B). The BHI shows high roughness, intermediate amplitude, and intense fracture features, which obliterated the identification of beddings [1]. The enlargement of fractures results in increased porosity, but the limited permeability suggests a lack of connectivity between pores. The thin section (X135m) is described as dolomite with quartz cement. It exhibits channel porosity and vugs, supporting the occurrence of enlarged fractures described in the BHI (Figure 6C).

Copyright© de Jesus IL et al.

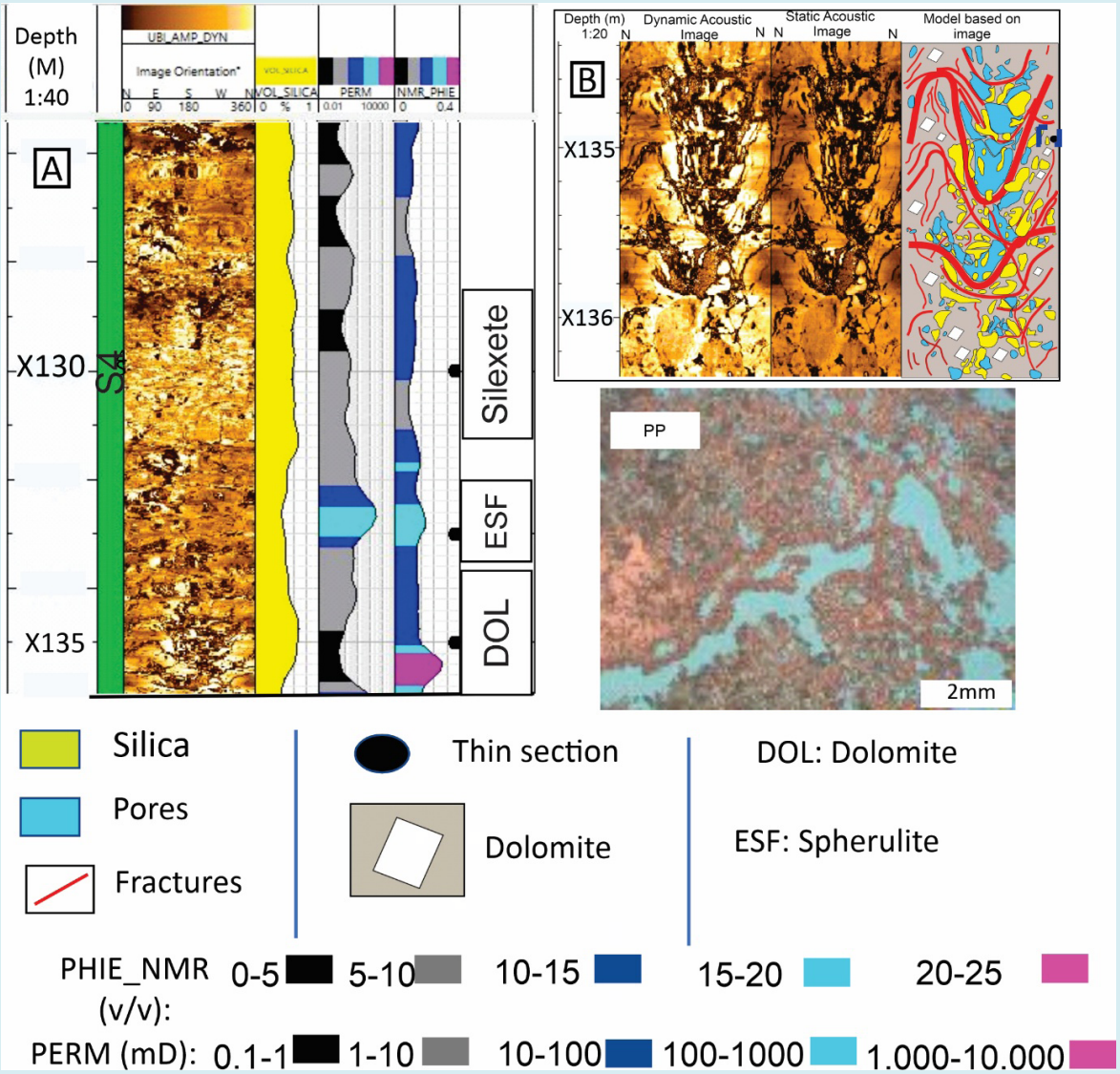


Figure 6: Segment of S4 zone. (A) 1) Depth; 2) Zone; 3) Acoustic BHI; 4) Silica volume; 5) Permeability; 6) Porosity; and 7) Lithology. (B) a Zoomed portion, indicated in the blue rectangle, 1) Depth; 2) Dynamic Image; 3) Static Image; 4) Model Based on image. (C) a thin section image.

The S5 zone has 51 meters (X001/X052m) and represents the top of the BVF. The GR presents a specific feature known as Lula Mark, consisting of nine GR pulses [18]. This is interpreted as short, intense episodes of lake-level variation (Figure 2). The Lula Mark is noticeable in several Santos Basin wells, indicating a regional characteristic [25]. This zone is characterized by a sudden decrease in silica and an increase in dolomite, possibly linked to the destabilization of Mg-clay and, hence, an increase in magnesium (Mg). The lack of microporosity in NMR T2 distribution confirms the absence of clay in the zone, with the accumulation of distribution to the right of the cutoff indicating an increase in free fluid (Figure 2). The BHI analysis, along with silica volume, suggests high and low-amplitude intercalation (Figure 7B). A common feature observed here is characterized by a uniform appearance, lack of structure, subtle roughness, low visual porosity, and the presence of breakouts, likely associated with post-depositional changes in cementation and silicification [3]. Additionally, intense dissolution is observed, characterized by low-amplitude pores and expressive high amplitude patches, which is interpreted as irregular silicification or intraclasts [1,3,33]. The thin section (X29.90) shows reworked particles, moderately sorted, mostly composed of spherulites, silica intraclasts, and quartz cement. The contact between particles indicates mechanical compaction (Figure 7C).

Copyright© de Jesus IL et al.

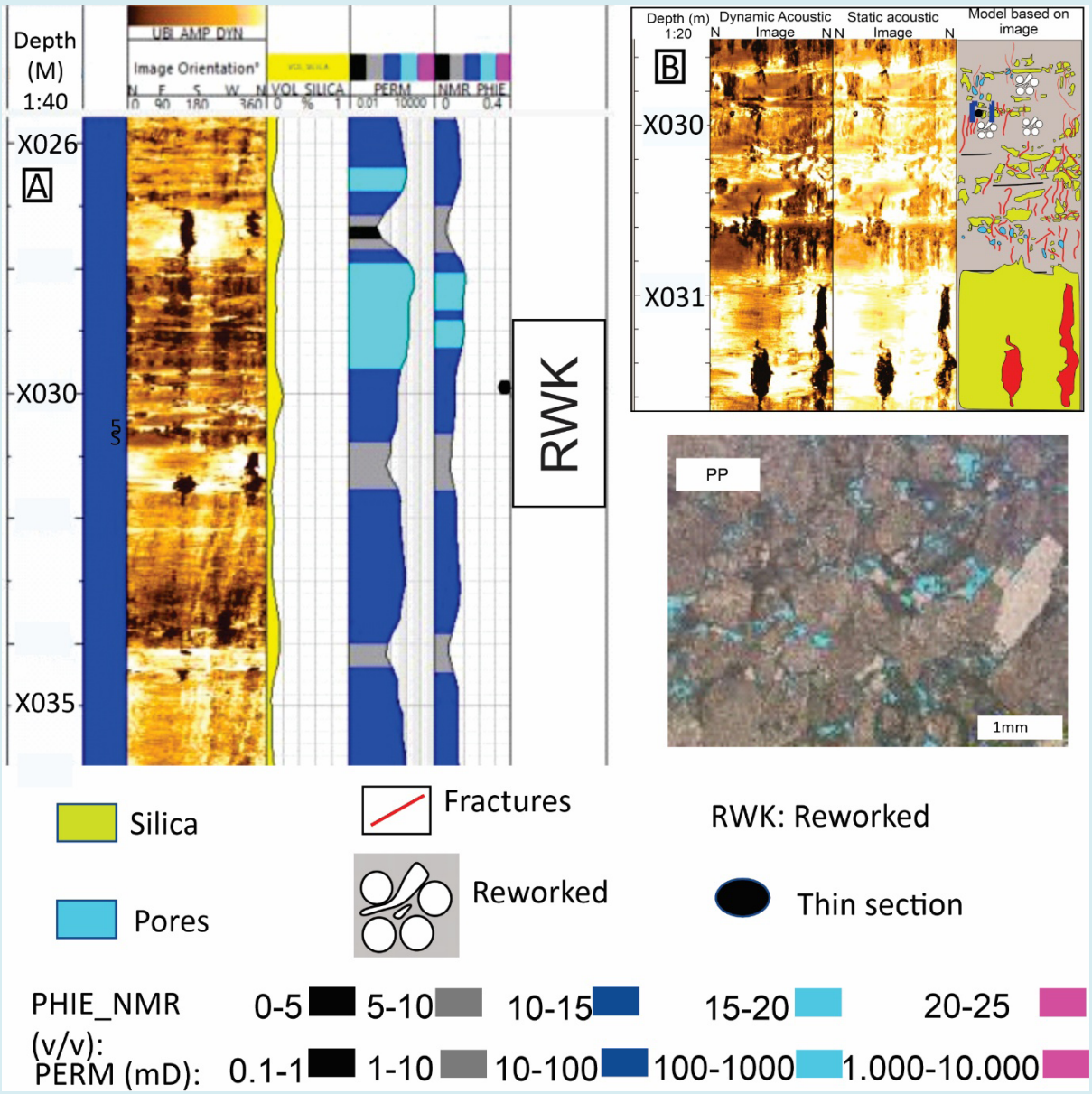


Figure 7: Segment of S5 zone. (A) 1) Depth; 2) Zone; 3) Acoustic BHI; 4) Silica volume; 5) Permeability; 6) Porosity; and 7) Lithology. (B) a zoomed portion, indicated in the blue rectangle, 1) Depth; 2) Dynamic Image; 3) Static Image; 4) Model Based on the image. (C) a thin section image.

After the crossplot analysis, the average porosity and permeability for the entire BVF and the five silica intervals were represented in pie charts (Figures 8 and 9). In the porosity domain, the BVF presents a predominance of high values (10-15%, Figure 8A). The S1 interval exhibits the best porosity values, with 54.9% falling in the very high porosity range (15-20%, Figure 8B). In contrast, the S3 interval has the lowest porosity values in the entire formation, with 55.7% falling into the moderate porosity range (5-10%, Figure 8C). It is worth noting that the S4 interval, characterized by a higher volume of silica, shows significantly high porosity values (59,7%, Figure 8E).

The permeability chart shows a predominance of high (10 to 100mD) and moderate (1 to 10m D) values for the entire BVF. Looking at the silica intervals individually, the S1 interval exhibits higher averages for high permeability (Figure 9B), while the S5 interval reaches approximately 83% when high and very high permeabilities are combined (Figure 9F). The S4 interval, on the other hand, highlights a predominance of low permeability values, with 47.2% falling into the moderate range and 11.3% into the low

Copyright© de Jesus IL et al.

range (Figure 9E). This might be associated with significant silicification during this interval, which likely contributed to pore cementation and compromising pore interconnectivity.

The relationship between the volumes of silica, dolomite and calcite was analyzed using a ternary plot (Figure 10). These volumes were estimated from elemental spectroscopy (ECS) logs based on silicon, magnesium, and calcium. The ternary plot (Figure 10) illustrates the mineralogical distribution of the main elements in the BVF. The S1 and S5 intervals have similar distributions, with high concentrations of calcite and low volumes of silica and dolomite. The S2 interval indicates a small distribution of silica, suggesting greater homogeneity in this volume. In turn, the S3 interval has a significant spread of silica volume and a smaller distribution of dolomite volume. Lastly, interval S4 illustrates the concentrated distribution of high silica volumes, highlighting intense silicification in this interval.

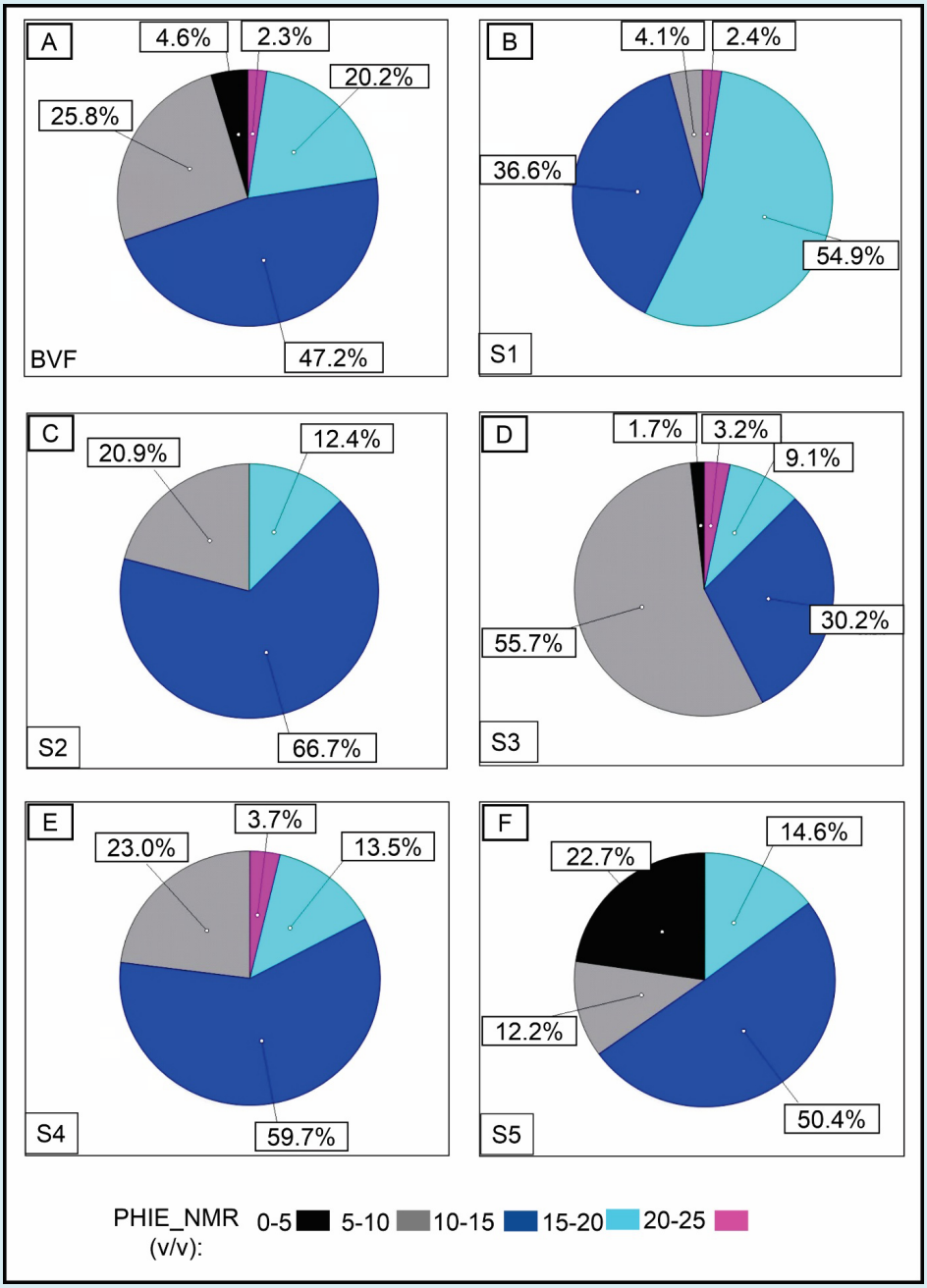


Figure 8: Pie charts displaying the average porosity distributions for the Barra Velha Formation (BVF; A) and the silica intervals (B-F).

Copyright© de Jesus IL et al.

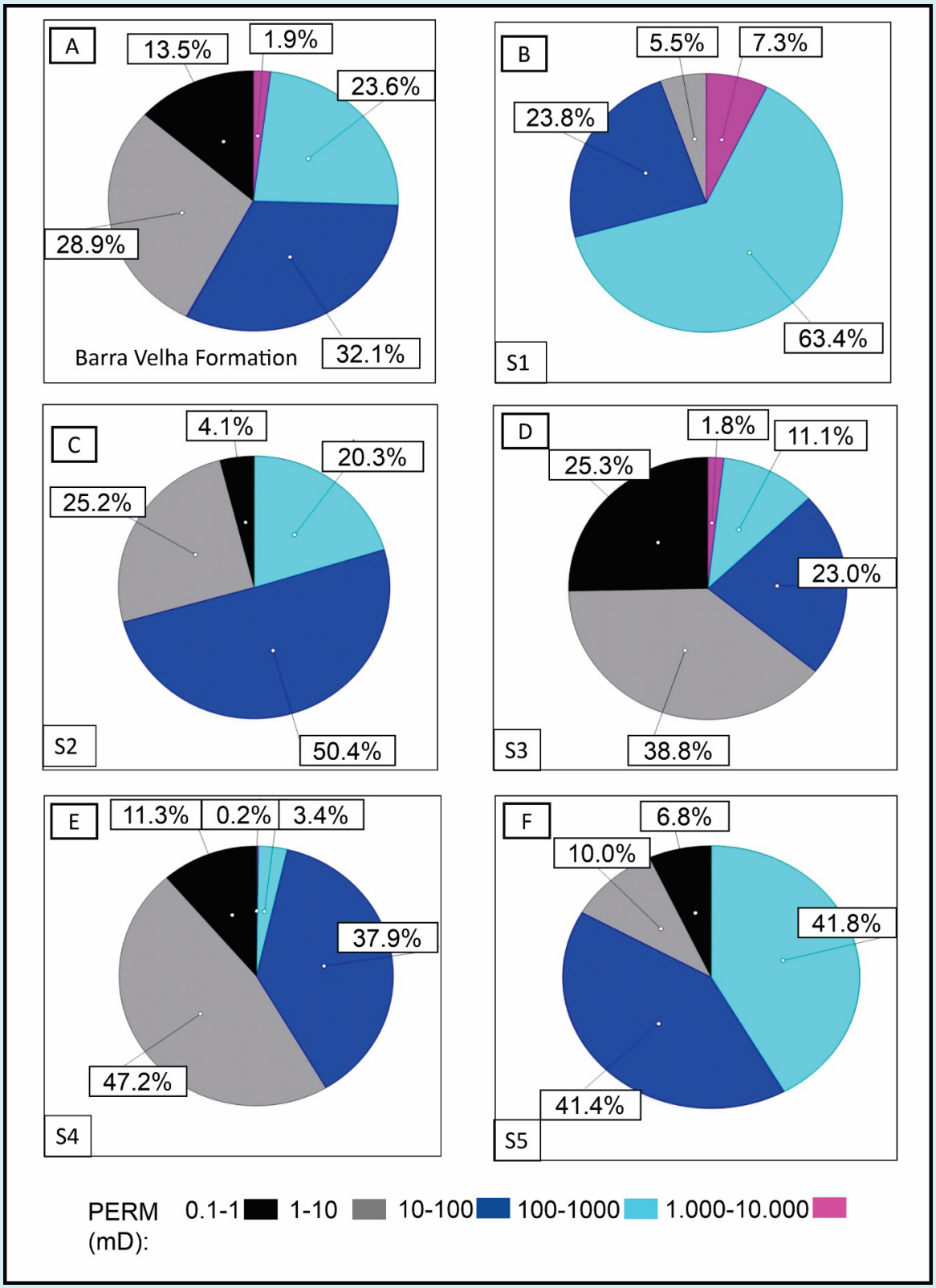


Figure 9: Pie charts displaying the average permeability distributions for the Barra Velha Formation (BVF; A) and the silica intervals (B-F).

Copyright© de Jesus IL et al.

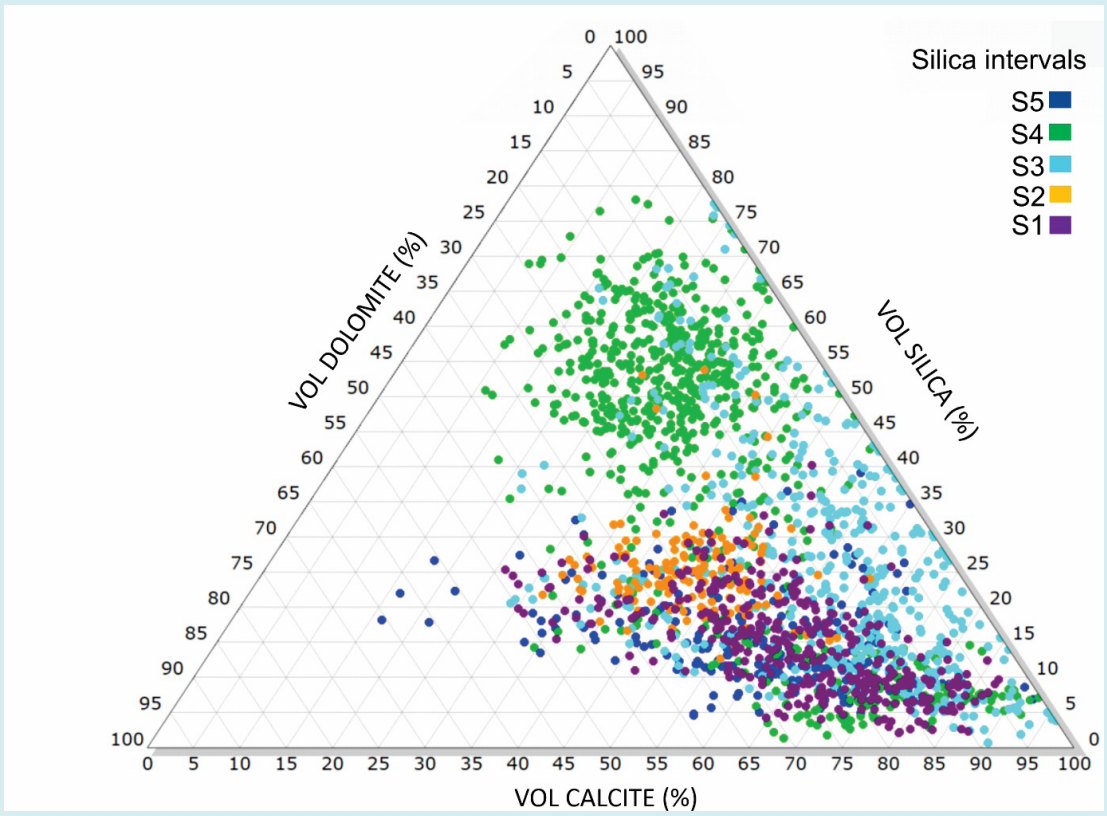


Figure 10: Ternary plot of silica, dolomite and calcite volumes for the Barra Velha Formation.

Discussions

Pre-Salt Carbonate Rocks Silicification: Diagenetic Effects and Permoporosity Alterations

The carbonate silicification process involves the replacement of carbonate constituents by silica (such as opal and quartz), in addition to the complete or partial filling of pore spaces [10,11] This diagenetic process can significantly modify sedimentary rocks at various phases of burial, ranging from early diagenesis, which is strongly influenced by depositional processes, to depths of several kilometers where mesodiagenetic and hydrothermal processes dominate [1,2,7,14,34,35,36].

Regarding the well study, the diagenetic silicification processes are evident through the elemental spectroscopy profile. By converting silicon concentration into silica volume (Equation 1), it was possible to establish five silica intervals for well A based on the different patterns and behaviors observed in the studied well (Figure 2). The increase in silica volume and the reduction in permoporous properties from the base to the top of the succession were evident, except in the S5 interval of well A. In this interval, shortly after a significant increase in the proportion of silica in S4, a sudden change occurs, with a reduction in values in the upper portion of the well (Figures 2, 6, and 7). Although the results presented in this study are based on a single well, the methodology is currently being applied to several nearby wells to assess the reproducibility of the observed results. This ongoing work aims to identify consistent silicification patterns, evaluate their lateral continuity, and establish the spatial extent of the identified diagenetic intervals across the Barra Velha Formation.

The interpretation of the BHI favored the characterization of different behaviors for silicified and non-silicified intervals, as well as the identification of the textural aspects that allowed for the association of possible lithofacies [2,3,4,8,9]. By correlating BHI with silica volumes, it was possible to associate different silica contents with their respective diagenetic impact. Although there is a general tendency towards reduced porosity and permeability with increasing silica content from the base to the top of the succession, divergent behaviors were identified, characterized by an increase in silica and permoporous properties (Figures 3, 4, 5, 6, and 7).

The workflow developed for this study favor convert the element's proportion in lithological volume considering molecular weight and elements ratio. This can be helpful in

Copyright© de Jesus IL et al.

studies that do not have software to provide this convertion automatically

The predominant behavior observed throughout all analyzed intervals is the alternating presence of silicified and non-silicified layers (Figures 3 and 4). In acoustic BHI, silicified layers exhibit high amplitude and appear as bright colors. Conversely, non-silicified layers display low amplitude, appearing as dark colors, and are interpreted as layers with limited silicification and a higher prevalence of interconnected pores [2,3,8,38] (Figures 3, 4, 5, 6, and 7). This type of porosity varies in proportion, geometry, and size, resembling pores observed in a petrographic thin section. It is important to highlight that these low amplitude layers indicate high porosity and permeability in the NMR logs, suggesting the presence of interconnected vugs [2,3,38]. Another notable feature is the presence of high-amplitude patches within predominantly low-amplitude strata or irregular beds, exhibiting significant variation in geometry, size, and proportion (Figs 3b, 5b, 6b). This behavior is associated with the silicification of thick intraclasts or irregular silicification [2,8,39].

Due to the heterogeneity in the vertical distribution of silica, the BVF was divided into five intervals (Figure 2). In the S1 interval, which represents the basal portion of the succession, a low volume of silica is observed, with some silicified layers showing limited fractures within the strata. Moving on to the S2 and S4 intervals, there is a clear increase in silica and an increase in fractures that are not restricted to the silicified layers but rather cross the succession vertically (Figures 3, 4, 5, 6, 7). However, this increase in silica is not uniform. While in some segments, it occurs uniformly (S2 interval, Figure 4), in others, it presents an expressive alternation of high and low silica values (S3 interval, Figure 6).

It is important to note that in S4 interval, there is a substantial volume of silica and varying porosity from very good to excellent (Figure 2 and 6). This interval is characterized by intense silicification, fracturing and significant porosity, as identified through acoustic BHI and petrographic thin section analysis (Figure 6). Conversely, in the S5 interval, there is a significant reduction in silica volume and an increase in permoporous properties (Figure 7). However, there is no significant fracturing identified in the interval. Possibly, the contribution of silica in the S5 interval comes mainly from the destabilization of magnesian clay to the detriment of hydrothermal silica.

Petrographic studies can detail the distribution of silica in carbonates. Together with acoustic BHI and silica volume, these studies allow for better visualization of the increase or reduction of silicification in rocks. In the thin sections used in this study, micro-quartz cement is observed filling the interparticle porosity. This cementation occurs as a product of early diagenesis during wetter periods in lake environments, which favored more acidic pH conditions and silica precipitation [8,25,38,40].

In areas with higher silica content, the fractures open wider, from millimeters to centimeters (Figure 6C). This is clearly visible in the S4 interval of well A, where there is a significant increase in the volume of silica related to the presence of fractured intervals and intervals dominated by silexites (Figure 6C). Channel-type porosity can also be identified [41] (Figure 6C). Although the expressive porosity, there is a significant reduction in permeability, indicating low interconnectivity of pores in this interval.

Due to physical principle of BHI, NMR and ECS tools, their integration favors reduce uncertainty about silicification and/or dolomitization process in carbonate reservoir and their impact on permoporous quality. The BHI have especial importance in dissolution characterization, which seems to be useful for futures researches and oil industry. Petrographic analysis presents great value in validate logs interpretation.

The Factors that Control the Silicification Process in the BVE

The analysis of rock data and geophysical logs has revealed a direct relationship between diagenetic events of dissolution and silicification in the carbonates of the Barra Velha Formation. Diagenesis occurred intensely throughout the entire unit, presenting, in addition to levels of silicification and dissolution, dolomitization and intense recrystallization [9,16,17,25,43].

In the Barra Velha Formation and its chronocorrelated sections, commonly dissolved magnesian clays generate secondary porosity that can be filled by silica or dolomite [16,25,34,44-46]. The dissolution of these clays can be associated with two factors: (i) water input, changing the chemistry of the lake [15,16,28,47] and (ii) influx of CO_2 from hydrothermal activity [7,48]. These conditions apparently favored the reduction of pH (below 9), which compromised the stability of magnesian clays.

The influence of magnesian clays in the Barra Velha Formation is identified in different works [16,17,24,25,48,44,50]. These clays are typically associated with intervals showing low GR, high sonic values and low porosity [17]. Petrographic thin section analysis is commonly used for identifying Mg-clays. However, based on our data analysis, no intervals characterized by magnesian clays were observed in this study.

Copyright© de Jesus IL et al.

It is possible that the absence of magnesian clay in this study area is due to magmatic events that caused intrusions near the well-studied area, leading to an increase in CO_2. This increase in CO_2 may have reduced the alkalinity of the fluids of the Barra Velha Formation. Consequently, the instability of magnesian clays was generated, leading to their dissolution and release of Si and Mg during early diagenesis. These types of clay minerals are highly sensitive and unstable to changes in water pH [2,7,16,19,25,51,52].

In Pre-salt area, carbonate rocks present significant heterogeneity and diagenetic processes that result in large variations in porosity and permeability [34]. As a result, the porosity observed in the reservoir rocks appears to be predominantly secondary, resulting from the dissolution of pre-existing constituents. The hydrothermal alteration is concentrated near faults, fractures, and unconformities that act as ducts, favoring the carbonate dissolution, and consequently generating secondary porosity [7]. Also, the ascension of hydrothermal fluids favored silicification and dolomitization processes that act as an obliterator of porosity [1,7,8,30,52,53,54,].

The contribution of hydrothermal fluids to the diagenetic processes of dissolution and silicification is the subject of intense study [7,9,25,38,55,56]. The carbonate dissolution controlled by fracturing and deep burial can be significant enough to convert a carbonate reservoir with low porosity and permeability into a quality-producing reservoir, moderate to good, since there is a generation of vugular and intercrystalline porosity in the subsurface. In this case, the CO_2 derives from inorganic sources such as mantle degassing or magmatism [4,25,56]. The migration of fluids was facilitated by faults and the dense system of fractures, which are below seismic resolution, which acted as pipelines for CO_2 -rich fluids upwards. This rise contributed to the creation of vugs and led to the cementation of part of this porosity, dolomite, and quartz. Pyrite crystals, Barite and saddle dolomite were also identified as being associated with hydrothermal activity [7,38,57]. That said, it is possible to consider that hydrothermal dissolution played a relevant role in diagenetic processes due to a series of fractures and faults that acted as ducts for hydrothermal fluids, and consequently favored silicification, [4,55].

Conclusions

This study aimed to evaluate the impact of silicification diagenesis on the carbonate reservoirs of the Barra Velha Formation by integrating acoustic borehole image (BHI) data with elemental spectrometry. Based on the patterns and trends observed in the silica-volume logs, the Barra Velha Formation was subdivided into five intervals in Well A (S1, S2, S3, S4, and S5). These intervals served as the framework for all subsequent analyses conducted in this study.

The conversion of elemental proportions to lithological volumes, based on molecular weights and stoichiometric elemental ratios, proved to be an effective method for estimating mineral volumes. The BHI, NMR and ECS integration allowed a better understanding of silica impact on permoporous reservoir quality, while petrographic analysis granted logs interpretation validation.

The acoustic BHI log proved to be a powerful tool in identifying the rock's dissolution features and textural aspects based on the difference in amplitude. The tool's resolution allows it to identify details very close to those observed in rock data in lithological terms, which are then corroborated by rock data.

The integration of acoustic BHI and silica volume made it possible to correlate silicified spots using the amplitude difference. In this work, the acoustic BHI's high transit time amplitude was defined as a silicified (cemented) interval, while a low amplitude was characterized as a porous interval. This difference in amplitude corroborated the proposed difference between silicified and distributed intervals.

The porosity and permeability logs were reinforced into five low to excellent classes and associated with the acoustic BHI and silica volume logs. In this way, it was possible to infer the impacts of silicification on permoporous properties. This analysis identified an increase in silica volume from the base to the top in the Barra Velha Formation and the opposite trend in permoporosity: reduction from the base to the top. However, it was possible to identify some local anomalies to this trend, in which the increase in silica is associated with increased permoporous properties.

Finally, based on the analyses carried out and bibliographical research, it was possible to conclude that heated hydrothermal fluids rich in silica rose through faults and fractures throughout the studied interval, favoring the dissolution of carbonates, generating secondary porosity, followed by precipitation of silica that filled (partially or completely) the pores of the S1 to S4 intervals. This model was not replicated in the S5 interval due to the absence of fractures that prevented the migration and accumulation mechanism observed in the first four intervals of the other intervals. Consequently, there was not the same interaction between fluids and rocks in the S5 interval. This becomes evident by the sudden reduction in silica content observed in this interval and the absence of layers or lithological bodies that would act as a fluid barrier between intervals S4 and S5.

Copyright© de Jesus IL et al.

Acknowledgement

The results and interpretations of this paper are part of the first author's Ph.D. The authors acknowledge the Petroleum Nacional Agency (ANP) for the data provided, the Universidade Federal Fluminense (UFF) for providing facilities and infrastructure for this research, and Equinor for being the research sponsor.

Paper information

I.L.J.: Conceptualization, Data curation, Formal analysis, Investigation, Methodology, Visualization, and Writing—original draft. F.R.A. Jr.: Methodology, Supervision, Validation, Visualization, and Writing—review & Editing. W.M.L.: Funding acquisition, Project administration, Resources, Software, and Supervision.

Competing Interests

The authors declare that they have no competing interests.

References

1. De Jesus IL (2023) Impacto da silicificação na permoporosidade em reservatórios carbonáticos na Formação Barra Velha, Bacia de Santos. PhD Thesis, Universidade Federal Fluminense, Niterói, Rio de Janeiro, Brazil.

2. Fernández-Ibáñez F, Jones GD, Mimoun JG, Bowen GM, Simo JA, et al. (2022) Excess permeability in the Brazil Pre-Salt: Nonmatrix types, concepts, diagnostic indicators, and reservoir implications. AAPG Bull 106(4): 1-38.

3. Basso M, Souza JPP, Honorio BCZ, Melani LH, Chinelatto GF, et al. (2022) Acoustic image log facies and well log petrophysical evaluation of Barra Velha Formation carbonate reservoir from the Santos Basin, offshore Brazil. Carbonates Evaporites 37: 50.

4. Cembrani E, Schmidt J, Souza M, Dos Santos T, Schrank ABS, et al. (2025) Multi-stage silicification in the Aptian pre-salt reservoirs of the Santos Basin, Brazil: Lacustrine recirculation and hydrothermal processes of silica precipitation in continental carbonates. J Sediment Res 96: 41-64.

5. Pereira MJ, Macedo JM (1990) A Bacia de Santos: Perspectivas de uma Nova Provincia Petrolifera na Plataforma Continental Sudeste Brasileira. Bol Geociênc Petrobras 4(11): 3-11.

6. Rossetti LM, Lima EF, Waichel BL, Scherer CM, Barreto CJ (2014) Stratigraphical framework of basaltic lavas in Torres Syncline main valley, southern Parana-Etendeka Volcanic Province. J S Am Earth Sci 56: 409-421.

7. Lima BEM, De Ros LF (2019) Deposition, diagenetic and hydrothermal processes in Aptian Pre-Salt lacustrine carbonate reservoirs of the northern Campos Basin, offshore Brazil. Sediment Geol 383: 55-81.

8. Menchick JVF, Altenhofen SD, Trombetta MC, Dos Santos TC, Schrank ABS, et al. (2026) Petrographic characterization and diagenetic evolution of a carbonate interval of the Barra Velha Formation, Santos Basin, Brazil. Research Square v1. Springer.

9. Cembrani E, Rodrigues AG, De Ros LF (2026) Early silicification of continental carbonates: Processes, settings, and implications for the South Atlantic pre-salt. Earth-Sci Rev 281: 105634.

10. Tucker ME, Wright VP (1990) Carbonate Sedimentology. Blackwell Scientific, Cornwall.

11. Flügel E (2010) Microfacies of carbonate rocks: Analysis, interpretation and application. Springer, Berlin.

12. Moreira JLP, Madeira CV, Gil JA, Machado MAP (2007) Bacia de Santos. Bol Geociênc Petrobras 15(2): 531-549.

13. Carminatti M, Dias J, Wolf B (2009) From turbidites to carbonates: Breaking paradigms in deep waters. Offshore Technology Conference.

14. Turner S, Regelous M, Kelley S, Hawkesworth C, Mantovani M (1994) Magmatism and continental break-up in the South Atlantic: High precision 40Ar-39Ar geochronology. Earth Planet Sci Lett 121(3-4): 333-348.

15. Pietzsch R, Oliveira DM, Tedeschi LR, Neto JVQ, Figueiredo MF, et al. (2018) Palaeohydrology of the Lower Cretaceous pre-salt lacustrine system, from rift to post-rift phase, Santos Basin, Brazil. Palaeogeogr Palaeoclimatol Palaeoecol 507: 60-80.

16. Farias F, Szatmari P, Bahniuk A, França AB (2019) Evaporitic carbonates in the pre-salt of Santos Basin – Genesis and tectonic implications. Mar Pet Geol 105: 251-272.

17. Carvalho AMA, Hamon Y, De Souza Jr OG, Carramal NG, Collard N (2022) Facies and diagenesis distribution in an Aptian pre-salt carbonate reservoir of the Santos Basin, offshore Brazil: A comprehensive quantitative approach. Mar Pet Geol 141: 105708.

18. Wright VP, Barnett AJ (2017) Classifying reservoir carbonates when the status quo simply does not work:

Copyright© de Jesus IL et al.

A case study from the Cretaceous of the South Atlantic. AAPG Annual Conference and Exhibition, pp 108-121.

19. Szatmari P, Milani EJ (2016) Tectonic control of the oil-rich large igneous-carbonate-salt province of the South Atlantic rift. Mar Pet Geol 77: 567-596.

20. Fodor RV, McKee EH, Asmus HE (1984) K-Ar ages and the opening of the South Atlantic Ocean: Basaltic rocks from the Brazilian Margins. Mar Geol 54(1–2): M1-M8.

21. Rigoti CA (2015) Evolução tectônica da Bacia de Santos com ênfase na geometria crustal: Interpretação integrada de dados de sísmica de reflexão e refração, gravimetria e magnetometria. MSc Thesis, Universidade do Estado do Rio de Janeiro, Rio de Janeiro, RJ, Brazil.

22. Mohriak W, Szatmari P, Anjos SMCA (2008) Sal: Geologia e Tectonica. Exemplos nas Bacias Brasileiras. Terra Didat 4(1).

23. Allen PA, Allen JR (2013) Basin analysis: Principles and application to petroleum play assessment. 3rd(Edn.), John Wiley & Sons, pp: 640.

24. Wright VP, Barnett AJ (2015) An abiotic model for the development of textures in some South Atlantic Early Cretaceous lacustrine carbonates. In: Microbial Carbonates in Space and Time: Implications for Global Exploration and Production. Geological Society, London, pp: 209-219.

25. Wright VP (2022) The mantle, CO2 and the giant Aptian chemogenic lacustrine carbonate factory of the South Atlantic: Some carbonates are made, not born. Sedimentology 69(1): 47-73.

26. Buckley JP, Bosence D, Elders C (2015) Tectonic setting and stratigraphic architecture of an Early Cretaceous lacustrine carbonate platform, Sugar Loaf High Santos Basin, Brazil. Geological Society, London, Special Publications.

27. Neves IDA, Lupinacci WM, Ferreira DJA, Zambrini JPR, Oliveira LOA, et al. (2019) Pre-salt reservoirs of the Santos Basin: Cyclicity, electrofacies, and tectonic-sedimentary evolution. Interpretation 7(4): SH33-SH43.

28. Gomes JP, Bunevich RB, Tedeschi LR, Tucker ME, Whitaker FF (2020) Facies classification and patterns of lacustrine carbonate deposition of the Barra Velha Formation, Santos Basin, Brazilian Pre-salt. Mar Pet Geol 113: 104176.

29. Ferreira DJA, Dias RM, Lupinacci WM (2021) Seismic pattern classification integrated with permeability-porosity evaluation for reservoir characterization of presalt carbonates in the Buzios Field, Brazil. J Pet Sci Eng 201: 108441.

30. De Jesus IL, Lebre MBS, Carmo MCD, Fatah TYA, Freire AFM, et al. (2021) Analysis of silica content and acoustic impedance on the porosity and permeability in the Barra Velha Formation, Santos Basin. 17th International Congress of the Brazilian Geophysical Society and EXPOGEf.

31. Oliveira FVCRS, Gomes RTM, Roriz CED, Silva KMS, Toledo RC (2022) Lithology identification through X-Ray Fluorescence (XRF) analyses on drill cuttings while drilling in Santos Basin. SPE Annual Technical Conference and Exhibition, Houston, Texas, USA.

32. Gaillot P, Brewer T, Pezard P, Yeh E (2007) Borehole imaging tools principles and applications. Sci Drill 5.

33. Lai J, Wang G, Wang S, Cao J, Li M, et al. (2018) A review on the applications of image logs in structural analysis and sedimentary characterization. Mar Pet Geol 95: 139-166.

34. Herlinger R, Zambonato EE, De Ros LF (2017) Influence of diagenesis on the quality of Lower Cretaceous Pre-Salt lacustrine carbonate reservoirs from northern Campos Basin, offshore Brazil. J Sediment Res 87(12): 1285-1313.

35. Sartorato ACL (2018) Caracterização faciológica, estratigráfica e diagenética dos reservatórios carbonáticos da Formação Barra Velha, Bacia de Santos. MSc Thesis, Universidade do Estado do Rio de Janeiro, Rio de Janeiro, RJ, Brazil.

36. Lupinacci WM, Fatah TYA, Carmo MC, Freire AFM, Gamboa LAP (2023) Controls of fracturing on porosity in pre-salt carbonate reservoirs. Energy Geosci 4(2): 100146.

37. Lai J, Wang G, Wang S, Cao J, Li M, et al. (2018) A review on the applications of image logs in structural analysis and sedimentary characterization. Mar Pet Geol 95: 139-166.

38. Xu K, Yu B, Gong H, Ruan Z, Pan Y, et al. (2015) Carbonate reservoirs modified by magmatic intrusions in the Bachu area, Tarim Basin, NW China. Geosci Front 6(5): 779-790.

39. Klimchouk A (2009) Morphogenesis of hypogenic caves. Geomorphology 106(1-2): 100-117.

40. Sartorato ACL, Tonietto SN, Pereira E (2020) Silicification and dissolution features in the Brazilian Pre-salt Barra Velha Formation: Impacts in the reservoir quality and

Copyright© de Jesus IL et al.

insights for 3D geological modeling. Rio Oil and Gas Expo and Conference, pp: 68-69.

41. James NP, Choquette PW (1984) Diagenesis 5. Limestones: Introduction. Geosci Can 10(4): 159-161.

42. Herlinger RJ, Freitas NG, Anjos WD, De Ros LF (2020) Petrological and petrophysical implications of magnesian clays in Brazilian Presalt deposits. Proceedings of the SPWLA 61st Annual Logging Symposium, pp. 1-13.

43. De Ros LF (2021) Syngenetic, diagenetic and hydrothermal processes in the pre-salt sag section of Santos and Campos Basins. Second EAGE Conference on Pre-Salt Reservoir: From Exploration to Production.

44. Tosca NJ, Wright VP (2015) Diagenetic pathways linked to labile Mg-clays in lacustrine carbonate reservoirs: A model for the origin of secondary porosity in the Cretaceous Pre-Salt Barra Velha Formation, offshore Brazil. Geological Society, London, Special Publications 435(1): 33-46.

45. Menezes CP, Bezerra FHR, Balsamo F, Mozafari M, Vieira MM, et al. (2019) Hydrothermal silicification along faults affecting carbonate-sandstone units and its impact on reservoir quality, Potiguar Basin, Brazil. Mar Pet Geol 110: 198-217.

46. Netto PRA, Pozo M, Da Silva MD, Mexias AS, Goms MEB, et al. (2022) Authigenic Mg-clay assemblages in the Barra Velha Formation (Upper Cretaceous) from Santos Basin (Brazil): The role of syngenetic and diagenetic process. Appl Clay Sci 216: 106339.

47. Tosca NJ, Tutolo B, Wood RA, Huwald N (2018) Chemical constraints on carbonate sedimentation and fabric development, Barra Velha Formation, Santos Basin, Brazil. AAPG Search and Discovery Article 90323.

48. Vieira de Luca PH, Matias H, Carballo J, Sineva D, Pimentel GA, et al. (2017) Breaking barriers and paradigms in Pre-salt exploration: The Pão de Açúcar discovery (offshore Brazil). In: Merrill RK, Sternbach CA (Eds.), Giant Fields of the Decade 2000–2010. American Association of Petroleum Geologists, USA, pp: 177-194.

49. Tosca NJ, Wright VP (2014) The formation and diagenesis of Mg-clay minerals in lacustrine carbonate reservoirs. American Association of Petroleum Geologists Annual Convention and Exhibition, Houston, Texas, USA.

50. Castro TM, Lupinacci WM (2022) Comparison between conventional and NMR Approaches for formation evaluation of presalt interval in the Búzios Field, Santos Basin, Brazil. J Pet Sci Eng 208 (Part D): 109679.

51. Pinto VHG, Manatschal G, Karpoff AM, Ulrich M, Viana AR (2017) Seawater storage and element transfer associated with mantle serpentinization in magma-poor rifted margins: A quantitative approach. Earth Planet Sci Lett 459: 227-237.

52. Schrank CE, Jones MWM, Howard DL, Berger A, Herwegh M (2024) Micro-scale structural and chemical characterization of deformed rocks with simultaneous in-situ synchrotron X-ray fluorescence and backscatter diffraction mapping. Chemical Geology 645: 121886.

53. Carmo MC (2021) Reconhecimento de eletrofácies carbonáticas e interpretação deposicional e diagenética, com base em dois poços do Pré-sal da Bacia de Santos. Dissertação de Mestrado, Universidade Federal Fluminense, Brazil.

54. Lebre M (2021) Analysis of flow facies in the pre-salt interval of Santos Basin. MSc Thesis, Universidade Federal Fluminense, Niteroi, Rio de Janeiro, Brazil.

55. Packard JJ, Al-Aasm IS, Samson I, Berger Z, Davies JA (2001) Devonian hydrothermal chert reservoir: The 225 bcf Parkland field, British Columbia, Canada. AAPG Bull 85(1): 51-84.

56. Biehl BC, Reuning L, Schoenherr J, Lüders V, Kukla PA (2016) Impact of hydrothermal dolomitization and thermochemical sulfate reduction on secondary porosity creation in deeply buried carbonates: A case study from the Lower Saxony Basin, northwest Germany. AAPG Bull 100(4): 597-621.

57. Ehrenberg SN, Walderhaug O, Bjørlykke K (2012) Carbonate porosity creation by mesogenetic dissolution: Reality or illusion? AAPG Bull 96(2): 217-233.

Copyright© de Jesus IL et al.